Phase diagram, extended domain walls, and soft collective modes in a three-component fermionic superfluid

G. Catelani and E. A. Yuzbashyan

Center for Materials Theory, Department of Physics and Astronomy, Rutgers University, Piscataway, New Jersey 08854, USA
(Received 10 June 2008; published 23 September 2008)

We study the phase diagram of a three-component Fermi gas with weak attractive interactions, which shows three superfluid and one normal phases. At weak symmetry breaking between the components the existence of domain walls interpolating between two superfluids introduces a new length scale much larger than the coherence length of each superfluid. This, in particular, limits the applicability of the local density approximation in the trapped case, which we also discuss. In the same regime the system hosts soft collective modes with a mass much smaller than the energy gaps of individual superfluids. We derive their dispersion relations at zero and finite temperatures and demonstrate that their presence leads to a significant enhancement of fluctuations near the superfluid-normal transitions.

PACS number(s): 67.85.Fg, 67.85.Lm

I. INTRODUCTION

In Landau's approach to phase transitions, conventional superfluidity and superconductivity are characterized by a single complex order parameter. However, in certain instances a proper description of a superfluid within this approach requires the introduction of an order parameter with several complex components. For example, in the case of superfluidity in ^{3}He [1] the spin-triplet, p-wave pairing is described by nine coefficients, and three different superfluid phases are experimentally realized. Other examples include unconventional superconductivity [2] in heavy fermion compounds and color superconductivity in nuclear matter [3], where different phases could be realized depending on the chemical potentials—the two-flavor color superconductor and the color-flavor-locked phase. Many aspects of multicomponent superfluidity in these systems are understood only on a phenomenolnical level due to their intrinsic complexity. Atomic Fermi gases, on the other hand, provide a unique avenue to explore these phenomena in a highly controllable way, thanks to the tunability of the interactions between atoms. Multicomponent superfluidity in atomic fermions could be realized, for example, by trapping and cooling multiple hyperfine states of the same atomic species [4,5] or of different species [6].

Here we present a study of the phase diagram of a three-component Fermi gas with weak attractive interactions. In particular, we consider the situation in which the "color" symmetry between the components is broken due to differences in the interaction strengths or chemical potentials, while the masses are the same. This situation is relevant to possible experiments involving three hyperfine states of ^{6}Li atoms. We first develop a Ginzburg-Landau expansion for this system and use it to confirm the previous results [7–9] that there are four possible phases: the normal state and three superfluid states S_1, S_2, and S_3. In each of the superfluid states two out of three components are paired, while the third one is in a normal state. First-order phase transitions between different superfluid states can be driven by varying interaction strengths, chemical potentials, particle densities, or temperature. We construct the phase diagram in grand-canonical

and canonical ensembles at finite and zero temperatures, shown in Figs. 1–3 and 6; see also Refs. [8,9].

The canonical phase diagram at fixed temperature (Fig. 2) contains regions where the homogeneous state is unstable. When the particle densities are within these regions the two superfluid states phase separate, as expected for the first-order phase transition; see, e.g., [10]. We therefore explore the properties of domain walls between different superfluids; see Fig. 4. In particular, we explicitly determine the shape and the thickness ℓ of the domain walls in various regimes. The case of weak symmetry breaking between two compo-
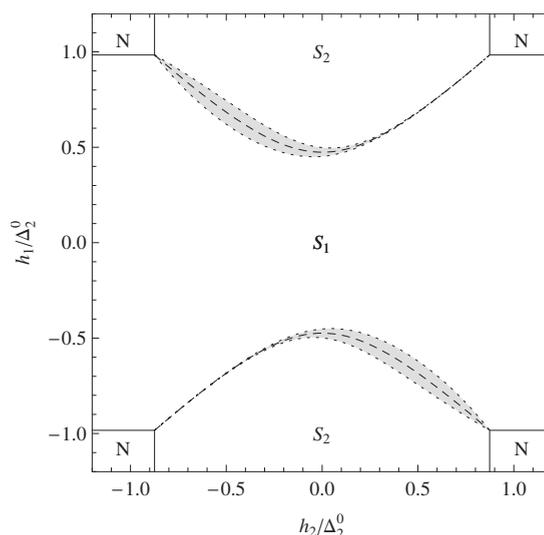

FIG. 1. Finite-temperature ($T=0.85T_{c_2}$) phase diagram for a three-component Fermi gas in the h_1-h_2 plane of chemical potential differences, Eq. (6). The two nonvanishing pairwise couplings $g_{1,2}$ are such that $T_{c_1}/T_{c_2}=1.04$, where T_{c_i} are defined below Eq. (10). Note that the normal state (N) is stable at large h_i while the superfluid states (S_i) at lower ones. The stronger interaction ($|g_1|>|g_2|$) determines the superfluid state (S_1) realized at $h_1=h_2=0$. The horizontal (vertical) segments denote second order N-S_1 (N-S_2) transitions. The dashed curves mark the first-order S_1-S_2 transitions; see Eq. (23). The shaded areas limited by the dotted curves [Eq. (22)] are the metastability regions.
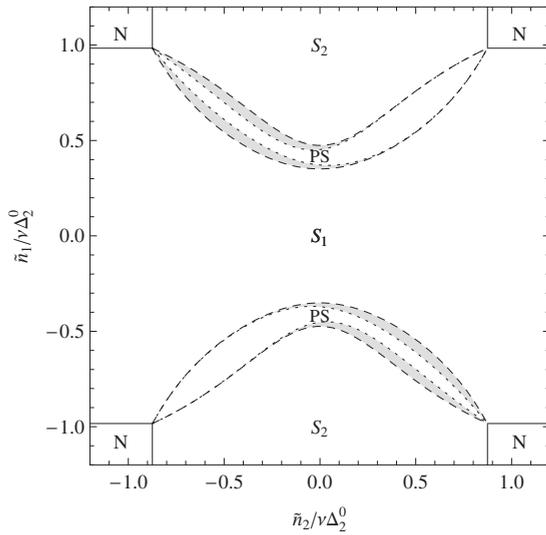
FIG. 2. Finite-temperature ($T=0.85T_{c_2}$) phase diagram for a three-component Fermi gas in the plane of particle density differences $\tilde{n}_1 - \tilde{n}_2$, Eq. (30). As in Fig. 1, the two nonvanishing pairwise couplings are chosen so that $T_{c_1}/T_{c_2}=1.04$. The horizontal (vertical) segments denote the second-order phase transition N-S_1 (N-S_2) between normal (N) and superfluid state S_1 (S_2). Dashed curves represent the limits of stability for the homogenous superfluids and enclose the phase-separated (PS) states. The shaded areas are the supercooling regions where a homogeneous superfluid state is metastable toward phase separation.
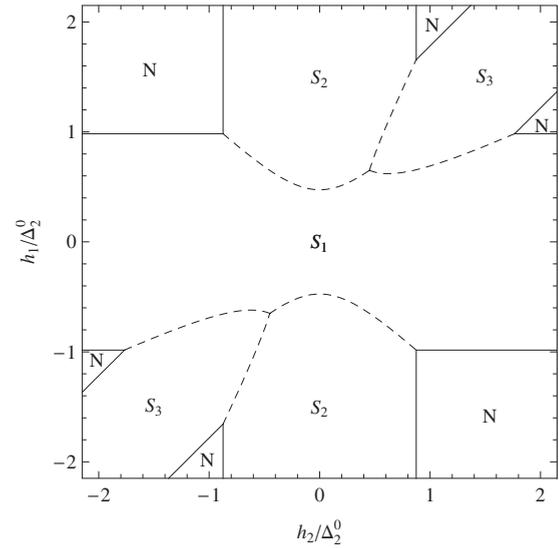

FIG. 3. Finite-temperature ($T=0.85T_{c_2}$) phase diagram for a three-component Fermi gas with pairwise attraction between components in the plane of chemical potential differences $h_1 - h_2$, Eq. (6). All three pairwise couplings are finite and such that $T_{c_1}/T_{c_2}=1.04$ and $T_{c_3}/T_{c_2}=0.97$. As in the case of only two nonvanishing couplings (cf. Fig. 1), we identify the regions where the normal state (N) and the superfluid states (S_i) are stable. The solid segments denote second-order N-S_i transitions. The dashed curves mark first-order S_i-S_j transitions. Note that at the two points where these curves meet all three superfluids can coexist.

nents (say, 1 and 2)—i.e., when the couplings of 1 and 2 with 3 and chemical potentials μ_1 and μ_2 are close—is especially interesting. At full symmetry between 1 and 2, $\ell=\infty$. This is natural as in this case the thermodynamic potential $\Omega(\Delta_1,\Delta_2)$, where Δ_1 and Δ_2 are the order parameters for superfluid states S_1 and S_2, respectively, is invariant with respect to rotations in the $\Delta_1 - \Delta_2$ space. This implies that the two minima of the potential $(\Delta_1,\Delta_2)=\{(\Delta_1^0,0),(0,\Delta_2^0)\}$ describing superfluids S_1 and S_2 can be connected by continuous lines of minima. Then, Δ_1 can be continuously deformed into Δ_2 at no energy cost when moving from one point in space to another. At weak symmetry breaking, as we demonstrate below, the thickness of the domain wall ℓ is parametrically larger than the coherence lengths ξ_1 and ξ_2 of superfluids S_1 and S_2.

For a trapped three-component gas the local density approximation (LDA) predicts sharp boundaries between superfluid states S_1 and S_2 [11]. In reality, there is a domain wall of length ℓ between S_1 and S_2 where the two superfluids coexist. Therefore, the characteristic length scale over which the boundaries predicted by the LDA are smeared is ℓ, rather than ξ_1 or ξ_2. Moreover, if the radius of the trap, R, is comparable to ℓ, the two superfluids coexist throughout the trap, so that the cases $R \gg \ell$ and $R \approx \ell$ are qualitatively different. In particular, this means that the LDA breaks down in the entire trap when $R \lesssim \ell$. For typical experimental parameters, the condition $R \gg \ell$ translates into $N_t \gg 10^4$ (see below), where N_t is the total number of fermions of all three species. Moreover, as we will see, the deviations from the LDA are significant already for N_t as large as 10^7.

Another consequence of the weak symmetry breaking discussed above is the presence of soft collective modes in mul-

ticomponent Fermi gases [7,12]. Suppose, for example, the system is in the superfluid state S_1. By considering the thermodynamic potential $\Omega(\Delta_1,\Delta_2)$ as above in the case of the domain wall, we expect fluctuations $\delta\Delta_2(\boldsymbol{r},t)$ towards superfluid S_2 to be massless in the symmetric case. Below we derive the mass and dispersion relations of the corresponding collective modes in the general asymmetric case at $T=0$ and at finite temperatures. We show that at weak symmetry
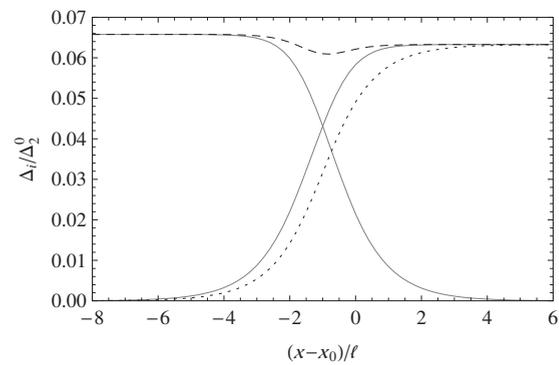

FIG. 4. Profiles of the order parameter components Δ_1 (decreasing solid line) and Δ_2 (increasing) in the presence of a domain wall between two superfluid states of a three-component Fermi gas. Here $T=0.92T_{c_2}$, $T_{c_1}/T_{c_2}=1.05$, and the chemical potential differences are $h_2/\Delta_2^0=-0.66$ and $h_1/\Delta_2^0 \simeq 0.84$, where T_{c_i} and Δ_i^0 are defined below Eq. (10). Note the overlap of the two components over the central region of size ℓ, Eq. (38). We also show the order parameter in the polar decomposition of Eq. (17); the dashed line is used for Δ and the dotted line for $\theta \times [0.063/(\pi/2)]$.

breaking the mass can be much smaller than the BCS gap in the superfluid S_1 in the absence of the third fermionic species. At finite temperature these fluctuations result, in particular, in an enhancement of the Ginzburg-Levanyuk number N_{Gi} by a large factor. In other words, the window of temperatures around the critical temperature for the normal-superfluid S_1 transition where fluctuations dominate becomes much larger in the presence of the third component.

Let us comment on the experimental realization of superfluidity in a three-component Fermi gas. Achieving a stable gas in this case appears more challenging than in a two-component one due to the enhanced role of the three-body scattering. In the two-component Fermi gas three-body recombination is suppressed thanks to the Pauli exclusion principle [13] and the system is stable over tens of seconds. In the three-component case there is no such suppression and the decay time is of the order of milliseconds [5]. Various proposals are being put forward in order to increase the life-time of the system, such as, e.g., the stabilization by an optical lattice [14] similar to that for bosonic atoms [15]. We note that the results presented in this paper are obtained in the weak-coupling regime, which is expected to be insensitive to the stabilization technique. For example, a lattice added to the trapping potential affects the single-fermion spectrum only. This is irrelevant at weak coupling since the superfluid energy scales are assumed to be much smaller than the fermionic bandwidth. The single-particle bands contribute only through the density of states at the Fermi energy irrespective of the details of the spectrum.

The paper is organized as follows. In the next section we give a brief overview of the mean-field approach and introduce our notation. In Sec. III we present the Ginzburg-Landau expansion of the thermodynamic potential and discuss the phase diagram at finite temperatures. We study the domain walls in Sec. IV, and in Sec. V we describe the zero-temperature phase diagram. Section VI is devoted to the collective modes. Finally, we summarize our results in Sec. VII.

II. THERMODYNAMIC POTENTIAL

In this section we outline the derivation of the thermodynamic potential, from which the phase diagram and all thermodynamic quantities can be obtained. We will not go into details, as the derivation is a well-known procedure [16]. Our starting point is the following Hamiltonian:

$$H = \sum_{i=1}^{3} \psi_i^\dagger H_0 \psi_i + H_{\text{int}}.$$ (1)

Here $H_0 = \mathbf{p}^2/(2m)$ is the single-particle Hamiltonian (we assume that all the particles have the same mass). As discussed in the Introduction, an optical lattice would modify the single-particle Hamiltonian. Its effect can be taken into account by introducing an effective mass $m_{\text{eff}} \neq m$, which in the weak-coupling regime results only in a renormalization of the density of states introduced below in Eq. (7). The pairwise interaction part is

$$H_{\text{int}} = \sum_{i,j,k,j',k'} \frac{g_i}{4} (\psi_j^\dagger \varepsilon_{ijk} \psi_k^\dagger)(\psi_{k'} \varepsilon_{ij'k'} \psi_{j'}),$$ (2)

where ε_{ijk} is the totally antisymmetric tensor and $\{i,j,k\} = \{1,2,3\}$. By the Hubbard-Stratonovich transformation, we introduce the pairing field $\vec{\Delta}(\tau,\mathbf{r}) = (\Delta_1(\tau,\mathbf{r}), \Delta_2(\tau,\mathbf{r}), \Delta_3(\tau,\mathbf{r}))$, and after integrating out the particle fields ψ_i, we obtain the following effective action for $\vec{\Delta}(\tau,\mathbf{r})$:

$$S_{\text{eff}}\{\vec{\Delta}\} = \int d\tau d^3x \left[\vec{\Delta}^\dagger \widehat{g^{-1}} \vec{\Delta} - \frac{1}{2} \ln \det \hat{G}^{-1} \right],$$ (3)

where $\hat{g}^{-1} = \text{diag}(g_i^{-1})$ and $\hat{G}^{-1}$ is the particles' inverse Green's function, which is a 6×6 matrix in Nambu-Gorkov space with the structure

$$\hat{G}^{-1} = \begin{pmatrix} (-\partial_\tau - H_0 + \mu_i)\delta_{ij} & \epsilon_{ijk}\Delta_k \\ -\epsilon_{ijk}\Delta_k^\dagger & (-\partial_\tau + H_0 - \mu_i)\delta_{ij} \end{pmatrix}.$$ (4)

Here μ_i are the chemical potentials for the different species.

In the mean-field approximation the thermodynamic potential is obtained by evaluating the effective action (3) for a τ-independent pairing field $\vec{\Delta}(\mathbf{r})$. This is expected to be an excellent approximation for the description of a weakly coupled fermionic superfluid at temperatures not extremely close to the transition temperature [10]. First, let us consider the case of a uniform order parameter. Performing a Fourier transform from real space-imaginary time to the momentum–Matsubara-frequency space in Eq. (3) we derive

$$\Omega = -\sum_i \frac{|\Delta_i|^2}{g_i} + \int \frac{d^3p}{(2\pi)^3} \left\{ \sum_i \frac{1}{2}\xi_i - \frac{1}{2\beta}\sum_n \right.$$
$$\times \ln\left[-2\prod_i (\omega_n^2 + \xi_i^2) + \sum_P (\omega_n^2 + \xi_i^2)|(\omega_n + i\xi_j)(\omega_n - i\xi_k) \right.$$
$$\left. + |\Delta_i|^2|^2 + \sum_P |\Delta_i|^2|\Delta_j|^2[(\omega_n + i\xi_i)(\omega_n - i\xi_j) + \text{c.c.}] \right] \right\},$$

(5)

where $\omega_n = 2\pi T(n+1/2)$, $\xi_i = \mathbf{p}^2/(2m) - \mu_i$, the sum over P denotes the sum over cyclic permutations of $\{i,j,k\} = \{1,2,3\}$, and "c.c." is the complex conjugate. For vanishing order parameter $\vec{\Delta} = 0$, we obtain the sum of the thermodynamic potentials for three perfect gases, as expected. Also, for an order parameter with only one nonvanishing component $\Delta_i \neq 0$, Eq. (5) reduces to the sum of the potentials of a normal gas and a two-component Fermi superfluid. Let us denote the corresponding zero-temperature order parameter of the two-component superfluid in the absence of the third fermionic species as Δ_i^0. We note that Eq. (5) is ultraviolet divergent, and a regularization procedure (e.g., a hard cutoff as for superconductors [10] or a T-matrix approach [17]) should be implemented. Then all physical quantities can be expressed in terms of the Δ_i^0's, as we do in what follows.

The (meta)stable states are given by the (local) minima of Ω. This condition determines the mean-field phase diagram. We will show below that the possible phases fall into two classes—normal state or a two component superfluid plus a

normal gas—in agreement with the results of [8,9]. The two superfluid components can be any two of the three atomic species; i.e., there are three possible superfluid states, which we denote as S_1, S_2, and S_3 when the paired species are 2 and 3, 1 and 3, and 1 and 2, respectively. For simplicity, unless otherwise specified, we assume from now on $g_3 = 0$, so that $\Delta_3 = 0$ and only Δ_1 and Δ_2 components of the order parameter can be nonzero. This can be a good approximation in the case of three hyperfine states of ^{6}Li, where two out of three Feshbach resonances mediating the attractive interactions between the states are close in magnetic fields [4]. The third resonance is at a lower field and can be neglected on the BCS side of the crossover. The inclusion of the case $g_3 \neq 0$ in our formalism is straightforward. We briefly comment on this case in Sec. III C and show the corresponding phase diagram in Fig. 3. For concreteness, we take $|g_1| > |g_2|$ and introduce the notation

$$h_1 = \mu_3 - \mu_2, \quad h_2 = \mu_3 - \mu_1, \tag{6}$$

for the differences in chemical potentials.

III. GINZBURG-LANDAU EXPANSION

Here we perform a Ginzburg-Landau expansion for the thermodynamic potential and use it to obtain the finite-temperature phase diagram of the system in the h_1-h_2 plane; see Fig. 1. We determine the superfluid-superfluid and superfluid-normal transition lines and the metastability regions in both grand-canonical (Fig. 1) and canonical (Fig. 2) ensembles. In the latter case there is a region of the phase diagram where a homogeneous state is unstable and a phase separation between two types of superfluid takes place. We identify this region as well as the corresponding supercooling lines; see Fig. 2.

According to Landau's phenomenological approach [10], the thermodynamic potential near a second-order phase transition can be expanded in powers of the order parameter. If only even powers are present and the coefficient of the fourth-order term is positive, the vanishing of the coefficient of the quadratic term determines the second-order transition point. When the fourth-order term also changes sign, the transition becomes first order, and higher-order terms should be included in the power series.

As shown by Gorkov [18], this phenomenological theory can be derived by expanding the microscopic theory in $|\vec{\Delta}|/2\pi T$ around $\vec{\Delta} = 0$. Using Eq. (3) [or Eq. (5) for the uniform part], we obtain to the fourth order in components of $\vec{\Delta} = (\Delta_1, \Delta_2, 0)$

$$\Omega - \Omega_N = \nu \sum_{i=1}^{2} \left\{ \alpha_i |\Delta_i|^2 + \frac{\beta_i}{2} \left[|\Delta_i|^4 + \frac{v_F^2}{3} |\nabla \Delta_i|^2 \right] \right\} + \nu \beta_{12} |\Delta_1|^2 |\Delta_2|^2, \tag{7}$$

where Ω_N is the normal-state thermodynamic potential of the ideal gas, ν is the density of states at the Fermi energy, and the coefficients α_i, β_i, and β_{12} are

$$\alpha_i = \ln \frac{T}{T_{c_i}} + \mathrm{Re}\, \Psi\left(\frac{1}{2} + i\frac{h_i}{4\pi T}\right) - \Psi\left(\frac{1}{2}\right), \tag{8}$$

$$\beta_i = -\frac{1}{4} \frac{1}{(2\pi T)^2} \mathrm{Re}\, \Psi''\left(\frac{1}{2} + i\frac{h_i}{4\pi T}\right), \tag{9}$$

and

$$\beta_{12} = \frac{1}{h_1 - h_2} \frac{1}{4\pi T} \mathrm{Im}\left[\Psi'\left(\frac{1}{2} + i\frac{h_2}{4\pi T}\right) - \Psi'\left(\frac{1}{2} + i\frac{h_1}{4\pi T}\right) \right]. \tag{10}$$

Here $\Psi(x)$ is the digamma function and T_{c_i} is the critical temperature of the superfluid S_i at zero chemical potential difference and in the absence of the third fermionic species—i.e., for $h_i = 0$ and $g_{j \neq i} = 0$. According to the standard BCS theory for two species, T_{c_i} is related to the corresponding zero-temperature order parameter Δ_i^0 as $T_{c_i} = e^{\gamma_E} \Delta_i^0 / \pi$, where γ_E is Euler's constant. Note that due to our choice $|g_1| > |g_2|$ for the coupling constants, $T_{c_1} > T_{c_2}$. We will comment below on the physical meaning of the temperatures T_{c_i} in the three species case.

Expressions (8)–(10) for the coefficients in the Ginzburg-Landau expansion (7) were derived in the weak-coupling limit, which enabled us to approximate the density of states with a constant ν. However, the structure of the potential (7) is dictated by symmetry and must remain the same at any coupling. Indeed, since the particle number is conserved separately for each species, the potential must be independent of the phases of the complex components of the order parameter. Therefore, the only allowed terms in the expansion to the fourth order are $|\Delta_i|^2$, $|\Delta_i|^4$, and $|\Delta_1|^2|\Delta_2|^2$.

The terms in curly brackets in Eq. (7) give the thermodynamic potential $\Omega_i(\Delta_i, h_i, T)$ of the two component superfluid S_i in the absence of the third species, while the $|\Delta_1|^2|\Delta_2|^2$ term represents the interaction between the two superfluids. The same expression for $\Omega_i(\Delta_i, h_i, T)$ was previously obtained [19] in a study of the nonuniform superconducting Fulde-Ferrell-Larkin-Ovchinnikov (FFLO) state [20]. In thin superconducting films in a parallel magnetic field the thermodynamic potential $\Omega_i(\Delta_i, h_i, T)$ describes the effect of the Zeeman splitting. In this case, h_i has a meaning of the Zeeman magnetic field and Δ_i is the superconducting order parameter. Let us briefly summarize the phases described by Ω_i in the h_i-T plane [21] before we proceed to the phase diagram for three species. For $T > T_{c_i}$ the quadratic coefficient is positive, $\alpha_i > 0$, and the two-component Fermi gas is in the normal state for any value of h_i. At temperatures $T_{\mathrm{tri}}^i < T < T_{c_i}$ a second-order transition to the superfluid state S_i takes place when $\alpha_i(h_i, T) = 0$. For temperatures lower than the tricritical temperature,

$$T_{\mathrm{tri}}^i \simeq 0.56 T_{c_i}, \quad i = 1, 2, \tag{11}$$

the quartic coefficient is negative, $\beta_i < 0$, whenever $\alpha_i \to 0$ and the normal-superfluid S_i transition is first order. The tricritical temperature and the corresponding tricritical chemical potential are determined from the condition $\alpha_i(h_{\mathrm{tri}}^i, T_{\mathrm{tri}}^i) = \beta_i(h_{\mathrm{tri}}^i, T_{\mathrm{tri}}^i) = 0$. This picture can also be obtained in the BCS limit from the phase diagram for polarized Fermi gases in the BCS-BEC crossover [22,23].

Now we turn to the analysis of general properties of the full thermodynamic potential for three species. The Ginzburg-Landau expansion (7) is a good approximation only when the polynomial $\beta_1|\Delta_1|^4 + \beta_2|\Delta_2|^4 + 2\beta_{12}|\Delta_1|^2|\Delta_2|^2$ is positively defined. Otherwise, $\Omega \to -\infty$ as $|\vec{\Delta}| \to \infty$ along a certain direction in the Δ_1-Δ_2 plane. Using Eqs. (9) and (10), one can show that this condition reduces to

$$\beta_i = -\frac{1}{4}\frac{1}{(2\pi T)^2} \, \mathrm{Re} \, \Psi''\left(\frac{1}{2} + i\frac{h_i}{4\pi T}\right) > 0, \quad i=1,2. \tag{12}$$

These inequalities are equivalent to $|h_i|/4\pi T \lesssim 0.304$. Since Eq. (7) was obtained by expanding in $|\vec{\Delta}|/2\pi T$, we also should have $|\vec{\Delta}|/2\pi T \ll 1$. Thus, the conditions of applicability of the expression (7) for the thermodynamic potential are

$$\frac{|h_i|}{4\pi T} \lesssim 0.304, \quad \frac{|\vec{\Delta}|}{2\pi T} \ll 1, \quad i=1,2. \tag{13}$$

It follows from the discussion in the previous paragraph that these inequalities hold only in the "high-temperature" regime $T > T_{\mathrm{tri}}^1 > T_{\mathrm{tri}}^2$. Otherwise, $\beta_1 < 0$ when $\Delta_1/2\pi T \ll 1$ and the first condition in Eq. (13) is violated. For the remainder of this section we restrict ourselves to this range of temperatures. Then, one can show using Eqs. (8) and (9) that the condition (12) always holds whenever any of the quadratic coefficients α_i is sufficiently small.

Let us discuss the possible phases of the three species system in the h_1-h_2 plane as a function of temperature going from higher to lower temperatures. For $T > T_{c_1} > T_{c_2}$ we see from Eq. (8) that both quadratic coefficients in Eq. (7) are positive, i.e.,

$$\alpha_i = \ln\frac{T}{T_{c_i}} + \mathrm{Re}\,\Psi\left(\frac{1}{2} + i\frac{h_i}{4\pi T}\right) - \Psi\left(\frac{1}{2}\right) > 0, \tag{14}$$

for any h_i and $i=1,2$. In this case, the only stable state is $\vec{\Delta}=0$—i.e., the normal state. As the temperature is lowered, α_1 first vanishes at $T = T_{c_1}$ and $h_1 = 0$, while α_2 remains positive. Therefore, a phase transition from the normal to the superfluid state S_1 occurs and T_{c_1} is the actual critical temperature for this transition. Generally, for $T_{c_2} < T < T_{c_1}$, we have $\alpha_2 > 0$, while α_1 changes sign at a temperature-dependent critical chemical potential $h_1^c(T)$ determined by the equation $\alpha_1(h_1^c(T), T) = 0$. At $h_1 < h_1^c(T)$ the superfluid state S_1 is the stable one, while at larger h_1 the system turns normal.

The case $T < T_{c_2}$ is more complicated. Now the conditions (14) hold for both components only when both $|h_1|$ and $|h_2|$ are sufficiently large. In the h_1-h_2 plane Eq. (14) determines four normal-state regions; see Fig. 1. A second-order phase transition from the normal to a superfluid state takes place when one of the coefficients α_i changes sign. For example, starting from the normal state, keeping h_2 fixed, and changing h_1, we get a transition between the normal state and the superfluid S_1, as α_1 becomes negative while α_2 is still positive. This argument, however, cannot predict the state of the system in the central region of the h_1-h_2 plane where both

α_i's are negative. We will explore this region in more detail in the following subsection.

A. Phase diagram in the vicinity of critical temperatures

As discussed above, the normal state is the stable phase in four sectors of the phase diagram, corresponding to the four corners in Fig. 1. Here we show that in the central region two different cases are possible: (i) the thermodynamic potential has only one minimum, which coincides with the superfluid state S_i for one of the two possible condensates Δ_i; (ii) Ω has two local minima, such that one condensate is the stable state and the other one is a metastable one. In the latter situation, a first-order phase transition separates the two superfluid states, as identified by the dashed lines in Fig. 1. The two minima are degenerate along these lines in the h_1-h_2 plane. The gray areas around the lines shown in Fig. 1 enclose the regions where two local minima are present.

In this subsection we obtain the phase diagram for the case when the two coupling constants g_1 and g_2 are sufficiently close in magnitude. We also take the temperature to be near the critical temperatures T_{c_2} and T_{c_1}, i.e.,

$$T_{c_1} - T_{c_2} \ll T_{c_2}, \quad T_{c_2} - T \ll T_{c_2}. \tag{15}$$

The first inequality in Eq. (15) holds since T_{c_i} is the critical temperature for the two component superfluid with coupling g_i [see the text below Eq. (10)] and the couplings are close. As we will see below, in this case the condition $|\vec{\Delta}|/2\pi T \ll 1$ for the validity of the Ginzburg-Landau expansion holds. Then, it follows from Eq. (13) that expression (7) for the thermodynamic potential can be used not just near the phase transition lines, but for all h_1 and h_2 such that $|h_i|/4\pi T \lesssim 0.304$. Nevertheless, the conclusions we draw regarding the phase diagram have general validity at sufficiently high temperatures $T > T_{\mathrm{tri}}^1 \simeq 0.56T_{c_1}$; see the text below Eq. (13) and at the end of this subsection.

Let us first consider a homogenous system; i.e., the gradient terms in Eq. (7) vanish:

$$\Omega(|\Delta_1|^2, |\Delta_2|^2) - \Omega_N = \nu \sum_{i=1}^{2} \left\{ \alpha_i|\Delta_i|^2 + \frac{\beta_i}{2}|\Delta_i|^4 \right\}$$
$$+ \nu\beta_{12}|\Delta_1|^2|\Delta_2|^2. \tag{16}$$

To find the stationary points of Ω, we pass to a polar coordinate representation

$$|\Delta_1| = \Delta\cos\theta, \quad |\Delta_2| = \Delta\sin\theta. \tag{17}$$

Differentiating Eq. (16) with respect to the angular variable θ, we find

$$0 = \Delta^2\cos\theta\sin\theta[\alpha_2 - \alpha_1 + \Delta^2((\beta_{12} - \beta_1)\cos^2\theta$$
$$+ (\beta_2 - \beta_{12})\sin^2\theta)], \tag{18}$$

where α_i, β_i, and β_{12} are defined by Eqs. (8)–(10), respectively. Equation (18) always admits the three solutions $\Delta = 0$, $\theta = 0$, and $\theta = \pi/2$. These are, respectively, the normal state, the condensate Δ_1, and the condensate Δ_2. To determine the value of the nonvanishing order parameter compo-

nent, we also need to equate to zero the derivative of the thermodynamic potential (16) with respect to Δ:

$$0 = \Delta[\alpha_1 \cos^2 \theta + \alpha_2 \sin^2 \theta + \Delta^2(\beta_1 \cos^4 \theta + \beta_2 \sin^4 \theta$$
$$+ 2\beta_{12} \cos^2 \theta \sin^2 \theta)]. \tag{19}$$

We obtain

$$\Delta_1^2 = -\alpha_1/\beta_1, \quad \Delta_2^2 = 0 \tag{20}$$

for $\theta = 0$ and

$$\Delta_1^2 = 0, \quad \Delta_2^2 = -\alpha_2/\beta_2 \tag{21}$$

for $\theta = \pi/2$. We see that $\Delta/(2\pi T)$ is indeed small near the second-order N-S_i phase transition, since $\alpha_i \rightarrow 0$ at the transition. This also implies that in the superfluid state S_i the chemical potential difference is such that $|h_i| \ll 4\pi T$, because the condition $|T - T_{c_i}| \ll T_{c_i}$, Eq. (15), makes the first term in the definition (8) of α_i small.

Having found the stationary points, we must check their stability. For a minimum, the second derivative must be positive. The second derivative of the thermodynamic potential (16) at stationary points (20) and (21) vanishes when

$$\alpha_i \beta_j - \alpha_j \beta_{12} = 0 \quad (i \neq j). \tag{22}$$

These equations define the stability lines enclosing the regions with two minima (gray areas in Fig. 1). Outside these regions, there is only one minimum, while the other stationary point is a saddle. Note that the fourth solution to Eq. (18) can be obtained by equating the terms in square brackets to zero. This solution is present only when the thermodynamic potential has two minima and corresponds to the saddle point between them.

Finally, the minima (20) and (21) are degenerate (the dashed lines in Fig. 1) when $\Omega(-\alpha_1/\beta_1, 0) = \Omega(0, -\alpha_2/\beta_2)$, which yields

$$\frac{\alpha_1^2}{\beta_1} = \frac{\alpha_2^2}{\beta_2}. \tag{23}$$

This condition can be satisfied only close to both second-order N-S_i transitions, so that $|h_i| \ll 4\pi T$ for both $i = 1$ and $i = 2$; see the discussion after Eq. (21). Substituting Eqs. (8) and (9) into Eq. (23) we obtain to leading order in $|h_i|/4\pi T$

$$\left[-\frac{1}{2} \Psi''\left(\frac{1}{2}\right) \right]\left(\frac{h_1^2 - h_2^2}{(4\pi T)^2}\right) = \ln \frac{T_{c_1}}{T_{c_2}}. \tag{24}$$

This equation shows that chemical potential differences, temperature, and the asymmetry in the interaction strengths determine the lines of the first-order phase transitions between different superfluid states. At fixed T, Eq. (24) defines transition lines $h_1(h_2)$ in the h_1-h_2 plane; see the dashed curves in Fig. 1.

In the presence of a trapping potential $V(\mathbf{r})$, we can combine our phase diagram of Fig. 1 with the so-called LDA [17] to predict the formation of different superfluid shells in the trap. The LDA assumes position-dependent chemical potentials

$$\mu_i = \mu_i^0 - V(\mathbf{r}), \quad i = 1, 2, 3. \tag{25}$$

The differences $h_1 = \mu_3^0 - \mu_2^0$ and $h_2 = \mu_3^0 - \mu_1^0$ [see Eq. (6)] remain constant throughout the trap and identify a point $\vec{h} = (h_1, h_2)$ on the phase diagram (Fig. 1). The temperature $T_{c_i} \equiv T_{c_i}(\mu_i)$ depends on the chemical potential μ_i as in the standard BCS theory; see the text below Eq. (10). As μ_i decreases from the center to the edge of the trap, $T_{c_i}(\mu_i)$ also decreases. On the other hand, the positions of the lines in the phase diagram in Fig. 1 are determined by the values of $T_{c_i}(\mu_i)$; see, e.g., Eq. (24). Therefore, the "local" phase diagram—i.e., the phase diagram of the homogenous system that corresponds to the values of chemical potentials at a particular point $\mathbf{r}$ in the trap—changes, and as we move from its center towards the edge, the regions where the superfluids are stable become smaller due to the decrease in $T_{c_i}(\mu_i)$. The actual values of μ_i^0 and consequently h_i must be determined self-consistently by fixing particle numbers for species 1, 2, and 3. Depending on the position of the resulting point $\vec{h}$ in the local phase diagram at the trap center, different configurations are possible. For example, if $\vec{h}$ is in the S_1 region at the center, the evolution of the local phase diagram with the position $\mathbf{r}$ can bring this point into the N region or make it pass through the S_2 region first. These two possibilities correspond to a central superfluid S_1 core surrounded by a normal shell or a superfluid S_1 core followed by an S_2 shell and a normal shell farther out, respectively. If $\vec{h}$ is in the S_2 region at the trap center, on the other hand, we obtain a superfluid S_2 core surrounded by a normal shell. Alternatively, for low particle number the normal-state atoms of the noncondensed species could form a normal core overlapping with the superfluid one. This qualitative picture is in agreement with numerical results of [11]. However, as we will discuss at the end of Sec. IV, the LDA has rather limited applicability in the presence of an S_1-S_2 boundary.

Let us summarize our observations so far in this section about the possible phases and phase transitions in the homogeneous case. We saw that for $T > T_{c_1} > T_{c_2}$ the system is in the normal state N for any chemical potentials differences $h_1 = \mu_3 - \mu_2$ and $h_2 = \mu_3 - \mu_1$ (recall that we set the coupling constant g_3 between species 1 and 2 to zero, while $|g_1| > |g_2|$). A second-order phase transition to the superfluid state S_1 where species 2 and 3 condense first happens at $h_1 = 0$ and $T = T_{c_1}$ at arbitrary h_2. For $T_{c_2} < T < T_{c_1}$ the only possible states are the normal state and superfluid S_1. At lower temperatures $T < T_{c_2}$ three states can exist as shown in Fig. 1. A second-order transition from the normal state to superfluid S_2 first takes place at $T = T_{c_2}$, $h_2 = 0$, and sufficiently large $|h_1|$ (so that S_2 wins over S_1); see Fig. 1. The S_1-S_2 transition is always first order, while the N-S_2 and N-S_1 are both second order provided that the temperature is above the tricritical temperatures (11), i.e.,

$$T > \max\{T_{\text{tri}}^1, T_{\text{tri}}^2\} \equiv T_{\text{tri}}. \tag{26}$$

For $T < T_{\text{tri}}$ at least one of the transitions N-S_1 or N-S_2 becomes first order and the Ginzburg-Landau expansion (7) breaks down; see the discussion below Eq. (13).

B. Phase separation

In the previous subsections we analyzed the phase diagram in the grand-canonical ensemble. Here we consider the canonical ensemble; i.e., we fix the densities n_i of the three fermionic species.

The corresponding chemical potentials are found by solving the equation

$$n_i = -\frac{\partial \Omega}{\partial \mu_i}. \tag{27}$$

If the differences between the densities are large, the chemical potential differences are also large and the gas is in the normal state. Let us assume that the densities deviate little from an average density n_0,

$$n_i = n_0 + \delta n_i. \tag{28}$$

Then, density deviations can be written as the sum of a noninteracting term and a correction due to the presence of the superfluid:

$$\delta n_i = \nu \delta \mu_i - \frac{\partial \delta \Omega}{\partial \mu_i}, \tag{29}$$

where $\delta \mu_i = \mu_i - \mu_0$, $\delta \Omega = \Omega - \Omega_N$, and μ_0 is the chemical potential for a noninteracting gas with density n_0. In Eq. (29) we neglected finite-temperature corrections to the noninteracting contribution $\nu \delta \mu_i$ [24].

For example, if the system is in the superfluid state S_1, we find using Eqs. (29), (16), and (20):

$$\tilde{n}_1 \equiv n_3 - n_2 = \nu h_1 - 2\frac{\partial \delta \Omega_1}{\partial h_1},$$

$$\tilde{n}_2 \equiv n_3 - n_1 = \nu h_2, \tag{30}$$

where

$$\delta \Omega_1 = -\nu \frac{\alpha_1^2}{2\beta_1}. \tag{31}$$

Using similar equations for the homogenous superfluid S_2, we obtain the phase diagram presented in Fig. 2 by mapping the lines in the phase diagram in the $h_1 - h_2$ space of Fig. 1 onto the corresponding lines in the $\tilde{n}_1 - \tilde{n}_2$ space of density differences. In particular, we note that each first-order phase transition line in the upper and lower half planes of Fig. 1 (dashed lines) maps into two lines. Indeed, according to Eqs. (31) and (29), $\delta \Omega$ and therefore $\tilde{n}_1$ and $\tilde{n}_2$ are different on the two sides of the transition. This means that, as usual in the case of first-order phase transitions, there is a region in the phase diagram where no homogeneous state is stable and phase separation must occur. Between this region and the stable homogeneous superfluid states, there are supercooling regions (gray areas) where the homogeneous states are metastable towards phase separation. The limits of these regions are found by mapping the corresponding limiting metastability lines in the grand-canonical phase diagram (dotted curves in Fig. 1).

At the end of the previous subsection we argued that, within the LDA, the two superfluid states can coexist in a

trap. In this section we have shown that the transition between the two superfluids is necessarily accompanied by a jump in the density. In this sense, it is similar to the low-temperature transition between the superfluid and normal states in the polarized two-component gas [17]. In this system, the density jump signals a potential breakdown of the LDA on the length scale of the coherence length. There is also evidence that surface tension effects should be taken into account to explain the shape of the superfluid core in elongated traps [25]. In the present case of the S_1-S_2 transition there are two competing length scales (the two coherence lengths) that can affect the properties of the interface, which we study in the next section.

C. Phase diagram in the case when all three couplings are nonzero

Here we briefly discuss the case when the coupling constant g_3 between species 1 and 2 is also nonzero. Let $|g_3| < |g_2|$. Now, in addition to $T_{c_{1,2}}$ there is the third temperature scale T_{c_3}. Similarly to $T_{c_{1,2}}$, it is defined as the critical temperature of the superfluid with components 1 and 2 in the absence of 3. Further, additional terms containing $|\Delta_3|^2$ appear in the thermodynamic potential (16). The coefficient α_3 of $|\Delta_3|^2$ is defined by Eq. (8) with $h_3 = \mu_2 - \mu_1 = h_2 - h_1$. For $T > T_{c_3}$, we have $\alpha_3 > 0$ and the phase diagram in Fig. 1 is unchanged. For $T_{\text{tri}} < T < T_{c_3}$, new N-S_3 second-order phase transitions are possible as well as first-order transitions S_3-S_1 and S_3-S_2. A phase diagram with these transitions is shown in Fig. 3. Note that, since $h_3 = h_2 - h_1$ is not an independent parameter, the phase diagram for the general case $g_3 \neq 0$ can be plotted in the same $h_1 - h_2$ plane as before.

IV. DOMAIN WALL

Until now we considered a spatially uniform system where one of the phases occupies the entire space. On the other hand, we have seen in the previous section that for a certain range of densities phase separation of the two superfluids S_1 and S_2 occurs, as shown in Fig. 2. This implies the formation of domain walls between homogeneous phases. Similarly, domain walls must form at the boundaries between S_1 and S_2 in a trapped three-component gas; see the text below Eq. (25). Let us analyze the properties of the domain wall using a grand-canonical thermodynamic potential. Its minima that correspond to the homogenous states S_1 and S_2 far from the domain wall must be degenerate for the superfluids to coexist in between. Indeed, the entire phase-separated regions in the diagram in Fig. 2 correspond to the lines of degenerate minima in Fig. 1 (dashed curves). To obtain the domain wall solution, we need to retain the gradient terms in the thermodynamic potential, Eq. (7), and minimize it subject to appropriate boundary condition. We first consider temperatures close to the critical one and later extend our considerations to lower temperatures.

A. Domain walls at temperatures close to the critical ones

Here, as in Sec. III A, we assume that conditions (15) hold. As discussed below Eq. (23), in this case the chemical

potential differences are such that $|h_i|/4\pi T \ll 1$. Then, the prefactors in front of the gradient terms in Eq. (7) can both be approximated with

$$\xi_0^2 = \frac{7\zeta(3)}{12}\left(\frac{v_F}{2\pi T}\right)^2. \quad (32)$$

We note that we cannot neglect the small differences of order $(h_i/2\pi T)^2$ in the prefactors of the fourth-order terms β_i and β_{12}, as these differences enter into the equations that determine the value of the order parameter; see Eq. (18).

For simplicity, let us assume that the translational invariance is broken only along the x axis, so that the system is in the homogeneous state S_1 at $x \to -\infty$ and in the state S_2 at $x \to +\infty$. According to Eqs. (20) and (21), this means $\theta \to 0$ for $x \to -\infty$, $\theta \to \pi/2$ for $x \to +\infty$, and $d\theta/dx \to 0$ for $x \to \pm\infty$. The minimization of the thermodynamic potential (7) yields a system of two second-order nonlinear differential equations for $\Delta(x)$ and $\theta(x)$ defined in Eq. (17). These equations admit a first integral, the conserved "energy" of the domain wall:

$$-\xi_0^2(\nabla\Delta)^2 - \xi_0^2\Delta^2(\nabla\theta)^2 + \Delta^2(\alpha_1\cos^2\theta + \alpha_2\sin^2\theta)$$
$$+ \frac{\Delta^4}{2}(\beta_1\cos^4\theta + \beta_2\sin^4\theta + 2\beta_{12}\cos^2\theta\sin^2\theta). \quad (33)$$

Our assumption (15) implies that the two homogenous states S_1 and S_2 have close values of the order parameter amplitude Δ; see Eqs. (20) and (21). This enables us to neglect the $(\nabla\Delta)^2$ term in Eq. (33). This term changes little on the length scale associated with the width of the domain wall, while the angular variable $\theta(x)$ changes by $\pi/2$ on the same length scale; i.e., the ratio of the $(\nabla\Delta)^2$ and $(\nabla\theta)^2$ terms in Eq. (33) is of order $(T_{c_1} - T_{c_2})/T_{c_1}$. Solving Eq. (19) for Δ in terms of θ and substituting the result into Eq. (33), we arrive at

$$\left[(\xi_0\nabla\theta)^2 - \frac{1}{2}(\alpha_1\cos^2\theta + \alpha_2\sin^2\theta)\right]$$
$$\times \frac{\alpha_1\cos^2\theta + \alpha_2\sin^2\theta}{\beta_1\cos^4\theta + \beta_2\sin^4\theta + 2\beta_{12}\cos^2\theta\sin^2\theta} = -S. \quad (34)$$

The value of the constant S on the right-hand side can be determined from the boundary conditions $\theta \to 0$ and $d\theta/dx \to 0$ as $x \to -\infty$:

$$S = \frac{\alpha_1^2}{2\beta_1}. \quad (35)$$

Note that νS is the condensation energy density for the homogenous state. Indeed substituting, e.g., Eq. (20) into Eq. (16) we obtain $\Omega_N - \Omega = \nu S$; see also Eq. (31).

Using Eq. (23), we rewrite Eq. (34) as

$$\frac{2d\theta}{dx} = \frac{1}{\ell}\frac{\sin 2\theta}{\sqrt{1 + a\cos 2\theta}}, \quad (36)$$

where

$$a = \frac{\alpha_1 - \alpha_2}{\alpha_1 + \alpha_2} \quad (37)$$

and

$$\ell^2 = \frac{1}{2}(\xi_1^2 + \xi_2^2)\eta^2. \quad (38)$$

Here we have introduced the coherence lengths of the two condensates,

$$\xi_i = \xi_0/\sqrt{-\alpha_i}, \quad i = 1,2, \quad (39)$$

and the scale factor

$$\eta^{-2} = \frac{\beta_{12}}{\sqrt{\beta_1\beta_2}} - 1, \quad (40)$$

where α_i, β_i, and β_{12} are defined by Eqs. (8)–(10), respectively. In particular, to leading order in $h_i/4\pi T$ we have

$$\eta \simeq \sqrt{12\frac{\Psi''\left(\frac{1}{2}\right)}{\Psi^{(4)}\left(\frac{1}{2}\right)}\frac{4\pi T}{h_1 - h_2}} \simeq 0.512\frac{4\pi T}{h_1 - h_2}. \quad (41)$$

From Eq. (36), we obtain an implicit equation for the spatial dependence of θ:

$$\frac{x - x_0}{\ell} = \sqrt{1-a}\,\text{arctanh}\left[\sqrt{\frac{1-a}{1+a\cos 2\theta}}\right]$$
$$- \sqrt{1+a}\,\text{arctanh}\left[\sqrt{\frac{1+a\cos 2\theta}{1+a}}\right]. \quad (42)$$

The parameters a and ℓ characterize the asymmetry of the domain wall with respect to reflection $(x-x_0) \to -(x-x_0)$ and its width, respectively. The parameter ℓ provides a new length scale, in addition to the coherence lengths, via the (large) parameter η; see Eq. (38). In the next subsection, we will see that the same parameter also enters the expression for the surface tension associated with the domain wall.

An example of the spatially nonuniform order parameters $\Delta_1(x)$ and $\Delta_2(x)$ in the presence of a domain wall is shown in Fig. 4. We also plot the angular variable $\theta(x)$ (rescaled) and the amplitude $\Delta(x)$. Note that $\Delta(x)$ shows little change. This is consistent with the assumption that gradients of $\Delta(x)$ can be neglected near the critical temperature T_{c_1}.

Finally, we note that because the densities on the two sides of the domain wall are different [see Eq. (30)], it could, in principle, be detected by imaging the sample. For bosonic atoms, overlap between two Bose-Einstein condensates was observed long ago [26] (for theoretical studies of the two-component bosonic system, see Ref. [27]). Alternatively, spatially resolved rf spectroscopy [28] could reveal the different gaps.

B. Surface tension

From the point of view of thermodynamic properties, the presence of a surface separating the two condensates can be

taken into account by including a surface tension term in the thermodynamic potential [10]. Moreover, as mentioned above, a proper treatment of surface tension effects is necessary to describe correctly the condensate profile in asymmetric traps [25].

The surface tension σ can be calculated by integrating the difference between the potential in the presence of the domain wall (Ω_{dw}) and the one in the uniform state (Ω_u) over the direction perpendicular to the domain wall:

$$\sigma = \int dx (\Omega_{dw} - \Omega_u). \tag{43}$$

Using Eq. (36), we derive

$$\sigma = \frac{2\nu S\ell}{\eta^2} \int d\theta \frac{4\sqrt{\beta_1\beta_2}\sqrt{1 + a\cos 2\theta}\sin 2\theta}{b_-\cos^2 2\theta + 2b_{12}\cos 2\theta + b_+}$$

$$\equiv \frac{2\nu S\ell}{\eta^2} f(a, \{\beta\}), \tag{44}$$

with S, ℓ, and η defined in Eqs. (35), (38), and (40), respectively,

$$b_\pm = \beta_1 + \beta_2 \pm 2\beta_{12}, \quad b_{12} = \beta_1 - \beta_2, \tag{45}$$

and β_1, β_2, and β_{12}, defined in Eqs. (9) and (10). Using these definitions and $h_i/4\pi T \ll 1$ [see the text below Eq. (23)], we estimate $b_+ \sim O(1)$, $\beta_i \sim O(1)$, $b_- \sim O(h^2/T^2)$, and $b_{12} \sim O(h^2/T^2)$. Therefore, we replace the denominator in the integral (44) by b_+ and obtain

$$f(a, \{\beta\}) \simeq \frac{1}{3a}[(\sqrt{1 + a})^3 - (\sqrt{1 - a})^3]. \tag{46}$$

By definition (37), the asymmetry parameter varies between -1 and 1. Therefore, $1 \geq f \geq 2^{3/2}/3 \simeq 0.94$. Neglecting this weak dependence on the asymmetry a, we can write

$$\sigma \simeq \nu S\sqrt{2(\xi_1^2 + \xi_2^2)}\eta^{-1}. \tag{47}$$

This expression shows that the surface tension is determined by the value of the condensation energy νS for the uniform system times the (root-mean-square) coherence length divided by the scale factor. As we will see in the next subsection, this formula for the surface tension is valid in a wider range of temperatures than the limiting case $T_{c_2} - T \ll T_{c_2}$ considered here.

C. Intermediate temperatures

In the preceding subsections we have considered a domain wall near the critical temperature. On the other hand, as discussed at the end of Sec. III A, the Ginzburg-Landau approach remains generally valid near second-order phase transitions even at lower temperatures above T_{tri}; see Eq. (26). So we can in principle analyze the properties of the domain wall at intermediate temperatures (and for larger differences in the critical temperatures than in the previous subsections). Approaching T_{tri}, the parameter β_1 becomes small by definition, while in the superfluid state α_1 is finite, so we expect the difference between Δ_1 and Δ_2 to grow; see Eqs. (20) and

(21). If this is the case, the approximation in which the gradient of Δ is neglected breaks down. To remedy this, we construct in this section a variational domain wall solution.

As a starting point for the variational approach, we note that the approximate domain wall solution is determined by three parameters: the position x_0, the asymmetry a, and the size ℓ. The first one cannot affect the energy (surface tension), as it only reflects the translational invariance of the infinite system, and henceforth we set $x_0 = 0$. In the (unphysical [29]) symmetric limit $a \to 0$, we can obtain an explicit expression for, e.g., the profile of Δ_1:

$$\Delta_1 = \Delta\sqrt{\frac{1}{2}\left[1 - \tanh\left(\frac{x}{\ell}\right)\right]}. \tag{48}$$

This suggests the following trial functions for the order parameters:

$$\Delta_i = \sqrt{\frac{-\alpha_i}{\beta_i}}\sqrt{\frac{1}{2}\left[1 \mp \tanh\left(\frac{x}{\ell_v} \mp \frac{\delta}{2}\right)\right]}, \tag{49}$$

where the Δ_i are fixed to their asymptotic values at $x \to \pm\infty$. We introduced a parameter δ which describes the overlap between the two superfluids and enables us to take into account the role of the interaction term in Eq. (7). As before, we also have a parameter ℓ_v related to the domain wall thickness [30]. Both parameters must be determined by minimizing the surface tension:

$$\sigma = \nu S\ell_v\left[-1 - \delta + \frac{\beta_{12}}{\sqrt{\beta_1\beta_2}}\delta(1 + \coth(\delta))\right] + \frac{\nu S}{2\ell_v}(\widetilde{\xi}_1^2 + \widetilde{\xi}_2^2), \tag{50}$$

with the coherence lengths

$$\widetilde{\xi}_i^2 = \frac{v_F^2}{3}\frac{\beta_i}{-\alpha_i}, \tag{51}$$

which reduce to Eq. (39) as $T \to T_{c_i}$.

After minimization, σ can be written as

$$\sigma = \nu S\sqrt{2(\widetilde{\xi}_1^2 + \widetilde{\xi}_2^2)}\eta_v^{-1}, \tag{52}$$

with the variational scale parameter given by

$$\eta_v^{-2} = \delta_0(1 + \coth(\delta_0))\frac{\beta_{12}}{\sqrt{\beta_1\beta_2}} - (1 + \delta_0), \tag{53}$$

where δ_0 is the solution to

$$\coth \delta_0 - \frac{\delta_0}{\sinh^2 \delta_0} + 1 = \frac{\sqrt{\beta_1\beta_2}}{\beta_{12}}. \tag{54}$$

Note that near the critical temperature, the right-hand side of the above equation tends to unity, so that $\delta_0 \to 0$ and $\eta_v \to \eta$. Since the variational approach gives an upper bound on the surface tension, it also gives a lower one on the domain wall thickness:

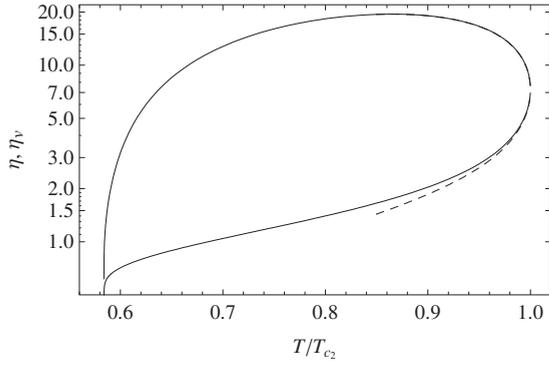$$\ell_v = \sqrt{\frac{1}{2}(\widetilde{\xi}_1^2 + \widetilde{\xi}_2^2)}\eta_v. \tag{55}$$

FIG. 5. Temperature dependence of the scale factors η_v (solid lines) and η (dashed lines) relating the domain wall size and the coherence lengths; see Eqs. (55) and (38). The coupling constants are chosen so that $T_{c_1}/T_{c_2} = 1.04$. The chemical potential differences h_i are the critical ones; see the text after Eq. (55). They have opposite signs for the lower curves [$h_1 = \pm h_1^c(T)$, $h_2 = \mp h_2^c(T)$] and the same sign for the upper ones [$h_1 = \pm h_1^c(T)$, $h_2 = \pm h_2^c(T)$]. In the latter case the difference between the two scale factors is not visible. Note that the scale factors are larger near T_{c_2} and/or for chemical potential differences of the same sign.

In Fig. 5 we compare the behavior of the scale factors η and η_v as functions of temperature for $T_{c_1}/T_{c_2} = 1.04$. The curves are computed in the two limiting cases in which the chemical potential differences h_i are the critical ones, $h_i = \pm h_i^c(T)$; cf. the discussion after Eq. (14). They correspond to the points where the first-order transition lines meet the second-order ones in Fig. 1. There are two inequivalent cases depending on the relative sign between h_1 and h_2. We choose these points in the phase diagrams because the Ginzburg-Landau expansion (7) is always valid in their vicinity as long as the temperature is above the tricritical temperature (26); see Sec. III. At fixed temperatures close to T_{c_2}, we find that the scale parameter η evolves smoothly as a function of the chemical potential differences along the first-order transition lines—i.e., going from one limiting case to the other one. Therefore, the limiting cases displayed in Fig. 5 give upper and lower bounds on the possible values of the variational scale parameter η_v.

Note that close to T_{c_2} the two parameters η_v and η have very similar values, and the approximate solution can be trusted in this regime. At smaller temperatures and chemical potential differences of opposite signs, the approximations made in the previous sections become invalid, and η decreases more rapidly than η_v. The latter remains of order unity at intermediate temperatures before quickly decreasing near T_{tri}^1. On the contrary, for chemical potential differences of the same sign, both approaches give similar results. Moreover, η_v initially *increases* with decreasing temperature, leading to potentially very thick domain walls with significant overlap between the two superfluid states. Again, when approaching T_{tri}^1 the scale parameter η_v quickly decreases. However, at these temperatures the present approach is invalid—higher orders in the Ginzburg-Landau expansion become relevant.

The above observations show the limits of applicability of the LDA (25) in the presence of a trap. For large η_v, the

surface tension is small, and we expect the density profiles to follow the shape of the trapping potential. On the other hand, in this case the width ℓ_v of the domain wall is large; see Eq. (55). The order parameter components vary smoothly on this scale and density jumps predicted by the LDA cannot be a good approximation of the actual density profiles. In other words, the LDA breaks down, not on a length scale $\tilde{\xi}_i$, as usually assumed, but on a much longer scale. In the opposite case of small η_v, the situation is reversed: the densities vary quickly on a length scale comparable to the coherence lengths. However, now the surface tension becomes important in asymmetric traps and the densities do not simply follow the profile of the trapping potential as in the LDA. This is seen, e.g., in the polarized two-component gas at low temperatures [25].

The above considerations are valid under the assumption than the sample size R is much larger than the domain wall thickness ℓ [31], in which case finite-size effects can be neglected. This requirement also limits the validity of the LDA. We can estimate how large, in terms of the number N of trapped atoms for each species, the sample should be in order to accommodate a domain wall. In the weak-coupling limit, a good estimate of the sample size is given by the Thomas-Fermi radius

$$R \simeq a_{ho}(48N)^{1/6}, \tag{56}$$

where $a_{ho} = \sqrt{1/m\omega_{ho}}$ is the harmonic oscillator length in the parabolic trap $V(r) = \frac{1}{2}m\omega_{ho}^2 r^2$. Next, we estimate the value of the coefficient ξ_0, Eq. (32), at $T \simeq T_{c_2}$ using

$$T_{c_2} \simeq 0.28 E_F e^{-\pi/2k_F|a_s|}, \tag{57}$$

where a_s is the (negative) scattering length and the Fermi momentum (at the trap center) is

$$k_F \simeq \frac{1}{a_{ho}}(48N)^{1/6}. \tag{58}$$

The previous three expressions (56)–(58) can be found in Ref. [17]. Substituting Eq. (57) into Eq. (32), we find

$$\xi_0 \simeq \frac{1}{k_F}e^{\pi/2k_F|a_s|}, \tag{59}$$

which is a lower bound for the coherence lengths defined in Eq. (39). Then, for ℓ, Eq. (38), we can write

$$\ell \gtrsim \frac{1}{k_F}e^{\pi/2k_F|a_s|}\eta. \tag{60}$$

For $k_F|a_s| \simeq 1$, the requirement $R/\ell \gg 1$ in terms of the total particle number $N_t \sim 3N$ becomes

$$N_t^{1/3} \gg 2\eta. \tag{61}$$

For a scale factor $\eta \sim 10$, this gives $N_t \gg 10^4$. However, due to the slow growth with N_t of the left-hand side of Eq. (61), even for a typical sample size with $N_t \sim 10^7$ [28] the ratio $R/\ell \sim 10$, and finite-size effects should be taken into account. Note that these estimates are also sensitive to the interaction strength $k_f|a_s|$ [cf. Eq. (59)], and for a weaker in-

teraction (e.g., $k_F|a_s| \simeq 0.5$) we obtain $N_t^{1/3} \gg 9\eta$ instead of Eq. (61) and $N_t \gg 10^6$.

V. PHASE DIAGRAM AT $T=0$

All our previous consideration have been restricted to the vicinity of second-order phase transitions and hence to the "high-temperature" regime $T > T_{tri}^1$. There is also a simple explicit description of the phase diagram at zero temperature, which we present in this section. In this case, all phase transitions (N-S_i and S_1-S_2) are first order, and the components of the order parameter $\vec{\Delta}$ at the minima of the thermodynamic potential are either zero or independent of the chemical potential differences [3]. Our phase diagram is in qualitative agreement with the numerical results of Refs. [8,32]. Although we consider the weak-coupling regime, we expect that our results will not qualitatively change at stronger coupling on the BCS side of the crossover. On the BEC side, on the other hand, the system behaves as a Bose-Fermi mixture (see, e.g., [33] for the two-component system) and we cannot exclude the possibility of qualitative differences (see also [34]). Finally, we note that in constructing the zero-temperature phase diagram we consider for simplicity only uniform states, neglecting the possibility that a spatially varying order parameter may be energetically favored in some regions of the phase diagram, as is the case for the FFLO state [20] in a two-component system [35]; see, e.g., Refs. [3,22,36–38].

According to Eq. (5), the differences $\delta\Omega_i$ between the thermodynamic potentials in the condensed and the normal states at the same chemical potentials is

$$\delta\Omega_i = -\frac{1}{2}|\Delta_i^0|^2 + \left(\frac{h_i}{2}\right)^2, \quad i=1,2. \tag{62}$$

Equating $\delta\Omega_i$ to zero, we obtain the first-order transition lines between superfluids S_i and the normal state (the Clogston-Chandrasekhar [39] critical field). The condition $\delta\Omega_1 = \delta\Omega_2$ yields the first-order transition line between the two condensates. These transitions are plotted as solid and dashed lines, respectively, in Fig. 6.

Considering as before the quadratic fluctuations [cf. Eq. (22); see also the next section], we determine the zero-temperature instability lines

$$h_j(h_i - h_j) = |\Delta_i^0|^2 - |\Delta_j^0|^2, \quad i,j=1,2, \tag{63}$$

for S_i becoming unstable towards S_j. Using these expressions, we obtain the (dotted) stability curves in the phase diagram shown in Fig. 6. The horizontal and vertical dotted lines indicate the instabilities of the superfluid states towards the normal state, which are identified by the conditions [3]

$$h_i = 2\Delta_i^0, \tag{64}$$

while the dash-dotted lines mark the instability of the normal state, obtained from the $T \to 0$ limit of Eq. (14):

$$h_i = \Delta_i^0. \tag{65}$$

The resulting zero-temperature phase diagram shown in Fig. 6 has a richer structure than that at "high" temperatures;
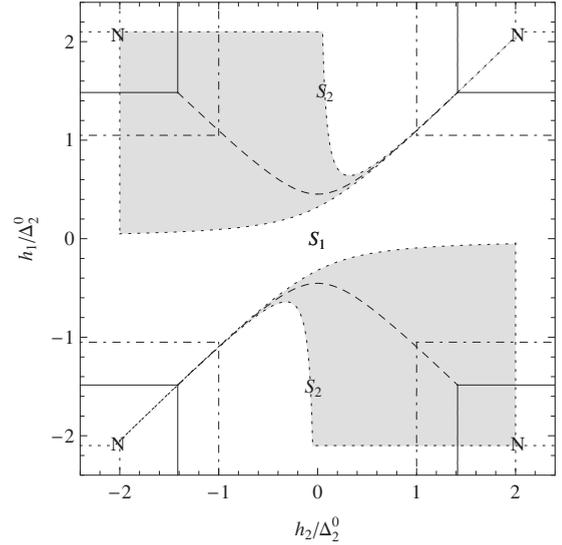

FIG. 6. Zero-temperature phase diagram for a three-component Fermi gas in the plane h_1-h_2 of chemical potential differences, Eq. (6). The two nonvanishing couplings constants are such that $\Delta_0^1/\Delta_0^2 = 1.05$, where Δ_0^i are defined below Eq. (5). As at high temperature (see Fig. 1), the normal state (N) is stable for large h_i. Horizontal (vertical) solid segments denote first-order N-S_1 (N-S_2) transitions between normal and superfluid states (in contrast, at high temperatures these transitions are second order). The dashed curves identify first-order S_1-S_2 transitions. The dotted curves represent the superfluid-state stability limits and the dot-dashed lines the normal-state stability limits. Shaded areas are regions where both superfluid states are (meta)stable. Note that these regions are much larger than the corresponding ones at high temperature in Fig. 1 and overlap with the normal-state stability regions.

see Fig. 1. For example, a larger region of the phase diagram is occupied by metastable states due to the first-order nature of the transition to the normal state. This in turn means that in the $\tilde{n}_1$-$\tilde{n}_2$ density-space phase-separated states occupy a larger region of the phase diagram. Consequently, more complicated domain wall structures are possible that interpolate between the different superfluid states and the normal state as well, as is the case for a two-component Fermi gas [25]. As remarked before, the phase separation translates into density jumps in the LDA treatment of the trapping potential. However, the validity of the LDA should be confirmed by estimating the effects of domain walls and surface tension, as in the finite-temperature case.

VI. COLLECTIVE MODES

In the absence of an external potential, the existence of thick domain walls is a manifestation of the presence of soft collective modes. While the former are possible only in the presence of degenerate ground states, the latter are a more general feature of the multicomponent Fermi gas. In this section we present the dispersion relations for these modes and comment on their role in limiting the applicability of the BCS mean-field approach. In trapped Fermi gases the collective modes are known to affect the experimentally accessible (hydrodynamiclike) response of the system [40].

For concreteness we assume that the ground state is the superfluid S_1 with homogeneous order parameter Δ_1 and consider small fluctuations around this state:

$$\Delta_1(\mathbf{r},t) = \Delta_1(1 + \psi(\mathbf{r},t))e^{i\phi(\mathbf{r},t)} + \delta\Delta_2(\mathbf{r},t). \quad (66)$$

The phase fluctuations described by ϕ correspond to the well-known soundlike Anderson-Bogoliubov mode [41], while the amplitude fluctuations ψ have a mass equal to $2\Delta_1$ [42]. These two modes have also been studied in the BCS-BEC crossover [43]. Here we are interested in the fluctuations $\delta\Delta_2(\mathbf{r},t)$ due to pairing in the noncondensed channel.

The propagator $D(\omega,q)$ of the $\delta\Delta_2(\mathbf{r},t)$ field is obtained by expanding Eq. (3) around the stationary point with $\Delta_1 \neq 0$, $\Delta_2=0$:

$$[\nu D(\omega,q)]^{-1} = \ln\frac{\Delta_1^0}{\Delta_2^0} + (\omega + h_1 - h_2)H(\omega,q;h_1,h_2)$$
$$+ J(\omega,q;h_1,h_2), \quad (67)$$

where functions H and J are given in the Appendix and Δ_i^0 are the values of the zero-temperature order parameter components; see the text below Eq. (3). Here we concentrate on the cases of zero temperature and vicinity to second-order phase transitions. Moreover, we consider only long-wavelength fluctuations—i.e., $q \to 0$.

A. Collective modes at $T=0$

In the limit $T \to 0$, the propagator in Eq. (67) becomes

$$[\nu D_0]^{-1} = \ln\frac{\Delta_1^0}{\Delta_2^0} + \mathcal{H}(\omega) + \left[(h_1 - h_2)\frac{1}{2}\frac{\partial^2}{\partial h_2^2} - \frac{\partial}{\partial h_2}\right]$$
$$\times \left(\frac{1}{h_1 - h_2}\mathcal{H}(0)\right)\frac{v_F^2 q^2}{3}, \quad (68)$$

with

$$\mathcal{H}(\omega) = \frac{1}{2}\ln\left[1 + \left(\frac{h_2 - h_1/2}{\Delta_1^0}\right)^2 - \left(\frac{\omega + h_1/2}{\Delta_1^0}\right)^2\right]. \quad (69)$$

Note that

$$[\nu D_0(0,0)]^{-1} \equiv \frac{1}{2}\ln[(\Delta_1^0)^2 + h_2^2 - h_2 h_1] - \ln\Delta_2^0 = 0$$
$$(70)$$

yields the stability condition (63) for $i=1$. Indeed, since the contribution of $\delta\Delta_2$ fluctuations to the action is $\delta\Delta_2^*(\omega,q)[D(\omega,q)]^{-1}\delta\Delta_2(\omega,q)$, the condition $[D(0,0)]^{-1} > 0$ determines the stability of the superfluid S_1 with respect to static uniform fluctuations.

Consider, e.g., the stability (or lack of it) of the superfluid S_1 with respect to shifts in the chemical potentials in the case of equal interaction strengths. For $h_1=0$ and small h_2 we get

$$[\nu D(0,0)]^{-1} \simeq \frac{1}{2}\left(\frac{h_2}{\Delta_1^0}\right)^2 > 0, \quad (71)$$

which shows that the superfluid S_1 is stable, as expected, since fluctuations toward condensation in the 1-3 channel

need to overcome the "Zeeman energy;" cf. Eq. (62). This is contrary to the claim in Ref. [12] that this chemical potential shift causes the system to become unstable. In contrast, for $h_2=0$ the inverse propagator $D(0,0)^{-1}$ is zero for any h_1, which indicates an instability. In this case the stable state is the superfluid S_2, as can be seen by repeating the above analysis with $1 \leftrightarrow 2$.

Now let us determine the dispersion relation of collective modes. For simplicity, we consider the case $h_1=0$. We have

$$\omega^2 = m^2 + v_0^2 q^2, \quad (72)$$

where

$$m^2 = (\Delta_1^0)^2 - (\Delta_2^0)^2 + h_2^2, \quad (73)$$

$$v_0^2 = \frac{v_F^2}{3}\left(\frac{\Delta_2^0}{\Delta_1^0}\right)^2 f\left(\frac{h_2}{\Delta_1^0}\right), \quad (74)$$

and

$$f(x) = \frac{1 - x^2}{(1 + x^2)^2}. \quad (75)$$

There are two branches with positive, $\omega > 0$, and negative, $\omega < 0$, energies. Similarly to the case of a polarized normal two-component gas [44], we can identify these excitations as bifermions and biholes. We note that the mass of these modes explicitly depends on symmetry breaking due to a difference in coupling constants [first two terms on the right-hand side of Eq. (73)] or chemical potentials. In the U(2)-symmetric case ($h_1=h_2=0$ and $g_1=g_2$, so $\Delta_1^0=\Delta_2^0$), the mass vanishes due to particle-hole symmetry. This result is independent of the weak-coupling assumption and holds at any coupling as long as particle-hole symmetry is present. Moreover, in the symmetric case the collective mode speed (74) reduces to the known result for the phase mode [41], $v_0 = v_F/\sqrt{3}$. In other words, in the symmetric limit in addition to the phase mode, there are two more modes with the same dispersion. This is expected in the framework of spontaneous symmetry breaking from U(2) down to U(1). Due to condensation into the superfluid state, the system is invariant only under rotations that change the phase of the order parameter and not under rotations transforming one of the components of $\vec{\Delta}=(\Delta_1,\Delta_2,0)$ into the other. Then, to the three broken generators correspond three massless Goldstone bosons. On the other hand, in the absence of particle-hole symmetry, the dispersion relation is modified [12], and two of the massless modes split into a massless mode with quadratic dispersion relation and a massive one [45].

B. Collective modes at finite temperatures

Let us consider the vicinity of the second-order phase transition N-S_1, so that $\Delta_1 \to 0$. In this case, the inverse propagator has a form similar to the quadratic term in the Ginzburg-Landau expansion (7) to which it reduces in the static limit $\omega \to 0$. For $\omega \neq 0$ the only difference is that the coefficients α_i, β_i, and β_{12} depend on ω. The frequency dependence of β_2 and β_{12} can be neglected since they multiply small quantities q^2 and $|\Delta_1|^2$, respectively. Using Eq. (3), we obtain

$$[\nu D(\omega, q)]^{-1} = \ln\left(\frac{T}{T_{c_2}}\right) + \frac{\beta_2}{2}\frac{v_F^2 q^2}{3} + \beta_{12}|\Delta_1|^2 - \Psi\left(\frac{1}{2}\right)$$
$$+ \frac{1}{2}\left[\Psi\left(\frac{1}{2} + \frac{-i(\omega + h_2)}{4\pi T}\right)\right.$$
$$\left. + \Psi\left(\frac{1}{2} + \frac{-i(\omega - h_2)}{4\pi T}\right)\right]. \quad (76)$$

The general structure of this propagator is the standard one for superconducting fluctuations [46], with overdamped fluctuations typical of the time-dependent Ginzburg-Landau approach. What is peculiar here is that the mass term is proportional to $|\Delta_1|^2$. This makes the decay of fluctuations in the 1-3 channel (i.e., towards superfluid S_2) faster than those toward the normal state. Nonetheless, they play an important role in causing deviations from mean-field theory. To show this, we employ the Ginzburg-Levanyuk criterion [10] for the simple case $h_1 = h_2 = 0$ and $T \lesssim T_{c_1}$.

As is well known in the theory of second-order phase transitions, fluctuations strongly modify the mean-field behavior at temperatures close to the critical one [10]. The temperature window around the critical temperature where the fluctuations dominate can be characterized by the Ginzburg-Levanyuk number N_{Gi}, so that for $\varepsilon \equiv |T - T_c|/T_c \gg N_{Gi}$ fluctuations are small. In three dimensions, due to amplitude fluctuations, $N_{Gi} \propto (T_c/E_F)^4$. This result can be obtained by writing the Ginzburg-Levanyuk criterion as [10]

$$\frac{T_c \chi}{\xi^3} \ll |\Delta|^2, \quad (77)$$

where

$$\chi \equiv D(0,0) \propto 1/\nu\varepsilon \quad (78)$$

is the pair susceptibility and

$$\xi^2 \equiv [D\partial^2 D^{-1}/\partial q^2](0,0) \propto v_F^2/T_c^2\varepsilon \quad (79)$$

is the coherence length squared. In both equations above the last term on the right is due to fluctuations of the order parameter Δ_1 itself, whose propagator has the form similar to Eq. (76) up to the replacement of indices $2 \rightarrow 1$, but without the term $\beta_{12}|\Delta_2|^2$; see [46]. Using $\nu \propto m^{3/2}E_F^{1/2}$ and $\Delta \propto T_c\sqrt{\varepsilon}$, we obtain $N_{Gi} \propto (T_c/E_F)^4$.

In the present case, we can use the same approach. Substituting the value of the order parameter Δ_1, Eq. (20), into Eq. (76) and using the definitions in Eqs. (78) and (79), we derive for the susceptibility and the coherence length

$$\chi \propto \left(\nu \ln\frac{T_{c_1}}{T_{c_2}}\right)^{-1}, \quad \xi \propto v_F\left(T_{c_1}\sqrt{\ln\frac{T_{c_1}}{T_{c_2}}}\right)^{-1}. \quad (80)$$

Using these expressions, we obtain for the three-component case

$$N_{Gi} \propto \left(\frac{T_{c_1}}{E_F}\right)^2 \sqrt{\ln\frac{T_{c_1}}{T_{c_2}}}. \quad (81)$$

We see that the fluctuations in the uncondensed (1)–(3) channel shrink the region of applicability of mean-field theory as

soon as $\ln T_{c_1}/T_{c_2} \gg (T_{c_1}/E_F)^4$—i.e., even for very small differences in the critical temperatures.

In the context of the BCS-BEC crossover, we recall that as the strength of the interaction grows, the ratio T_c/E_F grows too. This signals the breakdown of the mean-field approximation as the unitary limit is approached from the BCS side. The above estimate Eq. (81) for the Ginzburg-Levanyuk number indicates that this breakdown happens much sooner in the presence of a third interacting component.

VII. SUMMARY AND OPEN PROBLEMS

In this paper, we considered a three component (species) Fermi gas with attractive interactions between fermionic species in the weak-coupling regime. We confirmed that there are four possible homogeneous phases: the normal state (N) and superfluids S_i for $i = 1, 2,$ and 3 where species $j \neq i$ and $k \neq, i, j$ are paired. For simplicity, for most of the paper we restricted our analysis to the case when the components 1 and 2 do not interact with each other. In this case, the homogeneous phases of the system are N, S_1 (2 and 3 are paired), and S_2 (1 and 3 are paired). The extension of our findings to the general case of nonzero interaction between all components is straightforward; see Fig. 3 and Sec. III C.

We constructed the "high"-temperature $T > T_{tri}$ [see Eq. (11)] and zero-temperature phase diagrams for arbitrary differences between chemical potentials of the three species (Figs. 1 and 4). In particular, we identified the regions where different superfluid states and the normal state are (meta)stable and determined the lines of first-order S_1-S_2 and second-order N-S_1 and N-S_2 phase transitions. We also obtained the phase diagram in the canonical ensemble in the space of particle density differences ($n_3 - n_2$) and ($n_1 - n_3$) (Fig. 2). This phase diagram displays regions where the uniform superfluid states are unstable. Phase separation between superfluids S_1 and S_2 occurs for particle densities within these regions; i.e., the system becomes spatially inhomogeneous.

We analyzed the properties of the domain walls between superfluid states S_1 and S_2. The domain walls are present in the phase-separated region and at an interface between layers of S_1 and S_2 in a trapped three-component gas; see the text below Eq. (25). We determined the shape of the domain wall [see Fig. 5 and Eq. (42)] and demonstrated that its thickness ℓ, Eq. (38), provides a new length scale that can be parametrically larger than the coherence lengths $\xi_{1,2}$ of superfluids $S_{1,2}$, $\ell \gg \sqrt{\xi_1^2 + \xi_2^2}$. In particular, this means that the two order parameters of superfluids S_1 and S_2 can overlap significantly over extended regions of space. It also imposes severe restrictions on the LDA for evaluating the configuration of superfluid and normal layers in a trap [17]; see the discussion below Eq. (25) and in the end of Sec. IV C. The sharp boundaries between the superfluids predicted by the LDA have to be smeared over the length scale ℓ (rather than the coherence lengths ξ_1 or ξ_2). Furthermore, the LDA is valid only when the size of the trap, R, is much larger than the domain wall thickness, $R \gg \ell$. Otherwise, the two superfluids coexist throughout the trap. For experimentally attainable

systems, the condition $R \gg \ell$ translates into the total number of atoms $N_t \gg 10^4$ with corrections to the LDA being significant even for typical numbers in experiments, $N_t \sim 10^7$; see Eq. (61) and the text after it. We also evaluated the surface tension associated with the domain wall, Eqs. (47) and (52), which needs to be taken into account when considering the shape of the interface between superfluids S_1 and S_2.

Finally, we studied the collective modes (fluctuations) specific to our system in Sec. VI. Namely, in the superfluid state S_1 with order parameter Δ_1 there are fluctuations $\delta\Delta_2(\mathbf{r}, t)$ of the order parameter of superfluid S_2 and vice versa. We evaluated the mass and the dispersion relations of these collective modes at zero temperature and in the vicinity of the N-S_1 transition. At $T=0$ the mass is determined by perturbations that break the U(2) symmetry between species 1 and 2—the difference in chemical potentials and coupling constants for the interaction with 3. In the symmetric case the mass vanishes. At small symmetry breaking the collective modes soften and their mass can be parametrically smaller than the BCS energy gaps of superfluids S_1 and S_2. Similarly, near the critical temperature of the N-S_1 these fluctuations can significantly increase the Ginzburg-Levanyuk number [see Eq. (81)] in comparison to the two-component system. This indicates that stronger deviations from mean-field theory are possible in a three-component system.

The results outlined above were obtained in the weak-coupling BCS limit. A natural question is how they are modified in the BCS-BEC crossover regime and in particular at the unitary limit for two of the three components when the corresponding scattering length diverges. In the two-component case, there is a single length and energy scale at unitarity at $T=0$. This is not so in our case if the symmetry between the components is broken. Therefore, we expect qualitatively the same picture such as extended domain walls, soft modes, etc., as long as no true bound states are formed. It is also interesting to study these phenomena at lower temperatures close and below the tricritical temperature (26) which limits the applicability of our Ginzburg-Landau approach.

Let us also emphasize that to make more quantitative predictions about the possible experimental realization and detection of coexisting multiple superfluid states, it is necessary to go beyond or at least improve the LDA. Further work is also required to understand the effects of fluctuations in the unpaired channel on experimentally accessible quantities such as critical temperatures and the frequencies of collective oscillations in trapped gases in the hydrodynamic regime [47].

APPENDIX

In this appendix we present the expressions for the functions H and J introduced in Eq. (67) for the fluctuation propagator. The method to derive these functions is explained in [12]. So here we limit ourselves to the final results, which are straightforward extensions of those found in [12]:

$$H = \frac{1}{2\nu} \int \frac{d^3p}{(2\pi)^3} \frac{1}{2E_p} \left[\frac{1 - f(E_p - h_1/2) - f(\xi_{p-q} - h_1/2 + h_2)}{\omega - E_p - \xi_{p-q} + h_1 - h_2} - \frac{f(E_p + h_1/2) - f(\xi_{p-q} - h_1/2 + h_2)}{\omega + E_p - \xi_{p-q} + h_1 - h_2} + (q \to -q) \right], \quad (A1)$$

$$J = \frac{1}{2\nu} \int \frac{d^3p}{(2\pi)^3} \frac{\xi_p - \xi_{p-q}}{2E_p} \\ \times \left[\frac{1 - f(E_p - h_1/2) - f(\xi_{p-q} - h_1/2 + h_2)}{\omega - E_p - \xi_{p-q} + h_1 - h_2} - \frac{f(E_p + h_1/2) - f(\xi_{p-q} - h_1/2 + h_2)}{\omega + E_p - \xi_{p-q} + h_1 - h_2} \right] + (q \to -q),$$

$$(A2)$$

where

$$\xi_p = \frac{p^2}{2m} - \frac{\mu_2 + \mu_3}{2}, \quad E_p = \sqrt{\xi_p^2 + \Delta_1^2}. \quad (A3)$$

In the limit $h_i \to 0$, Eqs. (A1) and (A2) reduce (up to a normalization factor) to the functions H and J obtained in [12].

We note that in deriving, e.g., Eq. (68) we linearize the spectrum near the Fermi surface and assume particle-hole symmetry. Namely, we parametrize the momentum as $\mathbf{p} = \mathbf{n}(p_F + \xi/v_F)$, where p_F is the Fermi momentum, v_F the Fermi velocity, and $\mathbf{n}$ the unit vector on the Fermi sphere. Then, the integral over momentum is replaced with the integral over ξ and the vector $\mathbf{n}$:

$$\int \frac{d^3p}{(2\pi)^2} \to \nu \int d\xi \int \frac{d\mathbf{n}}{4\pi}, \quad (A4)$$

where ν is the density of states at the Fermi energy. Going beyond this approximation would enable the study of particle-hole asymmetry effects.

[1] A. J. Legget, Rev. Mod. Phys. **47**, 331 (1975).

[2] M. Sigrist and K. Ueda, Rev. Mod. Phys. **63**, 239 (1991).

[3] R. Casalbuoni and G. Nardulli, Rev. Mod. Phys. **76**, 263 (2004).

[4] M. Bartenstein *et al.*, Phys. Rev. Lett. **94**, 103201 (2005).

[5] C. H. Schunck, Y. Shin, A. Schirotzek, and W. Ketterle, Nature (London) **454**, 739 (2008).

[6] E. Wille *et al.*, Phys. Rev. Lett. **100**, 053201 (2008); M.

Taglieber, A.-C. Voigt, T. Aoki, T. W. Hänsch, and K. Dieckmann, Phys. Rev. Lett. **100**, 010401 (2008).

[7] C. Honerkamp and W. Hofstetter, Phys. Rev. Lett. **92**, 170403 (2004); Phys. Rev. B **70**, 094521 (2004).

[8] T. Paananen, J.-P. Martikainen, and P. Torma, Phys. Rev. A **73**, 053606 (2006).

[9] R. W. Cherng, G. Refael, and E. Demler, Phys. Rev. Lett. **99**, 130406 (2007).

[10] L. D. Landau and E. M. Lifshitz, *Statistical Physics* (Pergamon Press, Oxford, 1980), Pts. 1 and 2.

[11] T. Paananen, P. Torma, and J.-P. Martikainen, Phys. Rev. A **75**, 023622 (2007).

[12] L. He, M. Jin, and P. Zhuang, Phys. Rev. A **74**, 033604 (2006).

[13] D. S. Petrov, C. Salomon, and G. V. Shlyapnikov, Phys. Rev. Lett. **93**, 090404 (2004).

[14] V. Gurarie, unpublished.

[15] G. Thalhammer, K. Winkler, F. Lang, S. Schmid, R. Grimm, and J. Hecker Denschlag, Phys. Rev. Lett. **96**, 050402 (2006).

[16] See, for example, A. Altland and B. Simons, *Condensed Matter Field Theory* (Cambridge University Press, Cambridge, England, 2006).

[17] S. Giorgini, L. P. Pitaevskii, and S. Stringari, Rev. Mod. Phys. (to be published).

[18] L. P. Gorkov, Sov. Phys. JETP **9**, 1364 (1959).

[19] A. I. Buzdin, H. Kachkachi, Phys. Lett. A **225**, 341 (1997).

[20] P. Fulde and A. R. Ferrell, Phys. Rev. **135**, A550 (1964); A. I. Larkin and Y. N. Ovchinnikov, Zh. Eksp. Teor. Fiz. **47**, 1136 (1964); [Sov. Phys. JETP **20**, 762 (1965)].

[21] P. Fulde, Adv. Phys. **22**, 667 (1973).

[22] D. E. Sheehy and L. Radzihovsky, Phys. Rev. Lett. **96**, 060401 (2006); Ann. Phys. (N.Y.) **322**, 1790 (2007).

[23] M. M. Parish, F. M. Marchetti, A. Lamacraft, and B. D. Simons, Nat. Phys. **3**, 124 (2007).

[24] This approximation is valid when the chemical potential differences h_i are of the order of the critical ones (i.e., we are in the vicinity of the second-order phase transitions), and the temperature is not too close to the critical one $\ln(T_{c_2}/T) \gg (T_{c_2}/\mu_0)^2$.

[25] T. N. De Silva and E. J. Mueller, Phys. Rev. Lett. **97**, 070402 (2006).

[26] D. S. Hall, M. R. Matthews, J. R. Ensher, C. E. Wieman, and E. A. Cornell, Phys. Rev. Lett. **81**, 1539 (1998).

[27] R. A. Barankov, Phys. Rev. A **66**, 013612 (2002); B. Van Schaeybroeck, *ibid.* **78**, 023624 (2008).

[28] Y. Shin, C. H. Schunck, A. Schirotzek, and W. Ketterle, Phys. Rev. Lett. **99**, 090403 (2007).

[29] This limit is not physical because if $a = 0$, then $\alpha_1 = \alpha_2$, and by Eq. (23) $\beta_1 = \beta_2$. This requires $h_1 = \pm h_2$, which is compatible

with $\alpha_1 = \alpha_2$, only if $T_{c_1} = T_{c_2}$, while we assume $T_{c_1} > T_{c_2}$.

[30] For simplicity, we use the same length ℓ_v for both order parameters, which makes an analytical treatment possible. If the coherence lengths [see Eq. (51)] are vastly different ($|\tilde{\xi}_1 - \tilde{\xi}_2| \gg \tilde{\xi}_1 + \tilde{\xi}_2$), a better choice for the variational functions would employ two separate scales. However, for the estimates at the end of this section, the lower bound on the length scale found with this simpler treatment is sufficient.

[31] For the estimates we use the simpler high-temperature formulas of Sec. IV A. The results are unchanged if the variational results are used instead.

[32] H. Zhai, Phys. Rev. A **75**, 031603(R) (2007).

[33] P. Pieri and G. C. Strinati, Phys. Rev. Lett. **96**, 150404 (2006); Y. Shin, A. Schirotzek, C. H. Schunck, and W. Ketterle, e-print arXiv:0805.0623.

[34] P. F. Bedaque and J. P. D'Incao, e-print arXiv:cond-mat/0602525.

[35] We stress that, because of the "high-temperature" assumption, the FFLO state is not relevant to our study of the spatial variation of the order parameter due to a domain wall.

[36] T. Mizushima, K. Machida, and M. Ichioka, Phys. Rev. Lett. **94**, 060404 (2005).

[37] L. He, M. Jin, and P. Zhuang, Phys. Rev. B **73**, 214527 (2006).

[38] T. K. Koponen, T. Paananen, J.-P. Martikainen, and P. Torma, Phys. Rev. Lett. **99**, 120403 (2007).

[39] A. M. Clogston, Phys. Rev. Lett. **9**, 266 (1962); B. S. Chandrasekhar, Appl. Phys. Lett. **1**, 7 (1962).

[40] M. A. Baranov and D. S. Petrov, Phys. Rev. A **62**, 041601(R) (2000).

[41] P. W. Anderson, Phys. Rev. **112**, 1900 (1958); N. N. Bogoliubov, Nuovo Cimento **7**, 794 (1958).

[42] P. B. Littlewood and C. M. Varma, Phys. Rev. B **26**, 4883 (1982).

[43] J. R. Engelbrecht, M. Randeria, and C. A. R. Sá de Melo, Phys. Rev. B **55**, 15153 (1997).

[44] F. Fumarola, I. L. Aleiner, and B. L. Altshuler, e-print arXiv:cond-mat/0703003.

[45] We note that the dispersion relations presented in Ref. [12] are incorrect, as they predict for a collective mode the same dispersion relation as for free fermions; for positive and large chemical potentials, on the other hand, the mode velocity should be proportional to the Fermi velocity, as we show in the main text.

[46] A. Larkin and A. Varlamov, *Theory of Fluctuations in Superconductors* (Oxford University Press, Oxford, 2005).

[47] A. Altmeyer, S. Riedl, C. Kohstall, M. J. Wright, R. Geursen, M. Bartenstein, C. Chin, J. Hecker Denschlag, and R. Grimm, Phys. Rev. Lett. **98**, 040401 (2007).